nature water

Article

https://doi.org/10.1038/s44221-023-00152-y

Multifunctional solar water harvester with high transport selectivity and fouling rejection capacity

Received: 25 December 2022

Accepted: 2 October 2023

Published online: 30 October 2023

Check for updates

Xuanzhang Hao[1,2], Houze Yao[1,2], Panpan Zhang[1,2], Qihua Liao[1,2], Kaixuan Zhu[1,2], Jian Chang[3], Huhu Cheng[1,2] ✉, Jiayin Yuan[3] ✉ & Liangti Qu[1,2] ✉

Shortage of clean water continues to grow around the world, and the recent solar-powered interfacial system has emerged as a sustainable, efficient and CO_2-neutral approach to produce clean water. However, complex contaminants in surface water accompanied with environment pollution set huge obstacles for harvesting clean water via previous strategies. Here we develop a solar-powered graphene/alginate hydrogel (GAH)-based clean water extractor of super resistance to the transport of complex contaminants and ultra-antifouling capacity. This GAH features a high selectivity in water transport by rejecting >99.5% of volatile organic compounds, >99.3% of ions (Na^+, Mg^{2+}, K^+ and Ca^{2+}) and 100% of non-volatile organic compounds and bacteria; meanwhile, GAH is capable of rejecting oil adhesion by forming a large contact angle >140° under water, deactivating nearly 100% bacteria on surface and preventing salt crystallization. Given such promising adaptability to a wide environment, this GAH can directly convert surface water of complex components into safe drinkable water.

Upon rapid development of human society, surface water is continuously contaminated by complicated components from industrial emissions, including waste oils, volatile organic compounds (VOCs), heavy metal ions and microorganisms, just to name a few[1–3]. Meanwhile, shortage of clean water is becoming more and more serious, and one in three people currently does not have access to safe drinking water[4,5]. Traditional thermal distillation and membrane-based reverse osmosis technologies have been developed and in service for decades to separate water from the pollutants to meet the ever-growing standard of human life. However, the high energy consumption, complicated treatment processes, heavy economic burden and inevitable secondary pollution by operation-driven fuel combustions or waste membranes have restricted their practical applications in particular in developing countries and regions[6–9].

Solar-powered water production is considered as a green, sustainable and decentralized strategy to access clean water from seawater or undrinkable water, and could satisfy the urgent water demands around the world, because solar energy is a renewable energy that is inexhaustible, widespread and environmentally friendly[10–15]. Benefitting from the recent development of solar-powered interfacial materials such as graphene, polypyrrole and metal nanoparticles[16–21], considerable sunlight utilization efficiency and rapid vapour generation kinetics have been demonstrated. However, when complicated contaminants are present in surface water, the state-of-the-art single-function solar-powered system is far away from qualified devices that harvest water without hazardous components. For example, VOCs (for example, dichloromethane, toluene and phenol) widely distributed in surface water due to pollution are rather easy to transport through common

[1]Laboratory of Flexible Electronics Technology, Key Laboratory of Organic Optoelectronics & Molecular Engineering, Ministry of Education, Department of Chemistry, Tsinghua University, Beijing, P. R. China. [2]State Key Laboratory of Tribology in Advanced Equipment (SKLT), Department of Mechanical Engineering, Tsinghua University, Beijing, P. R. China. [3]Department of Materials and Environmental Chemistry, Stockholm University, Stockholm, Sweden. ✉e-mail: huhucheng@tsinghua.edu.cn; jiayin.yuan@mmk.su.se; lqu@mail.tsinghua.edu.cn

https://doi.org/10.1038/s44221-023-00152-y

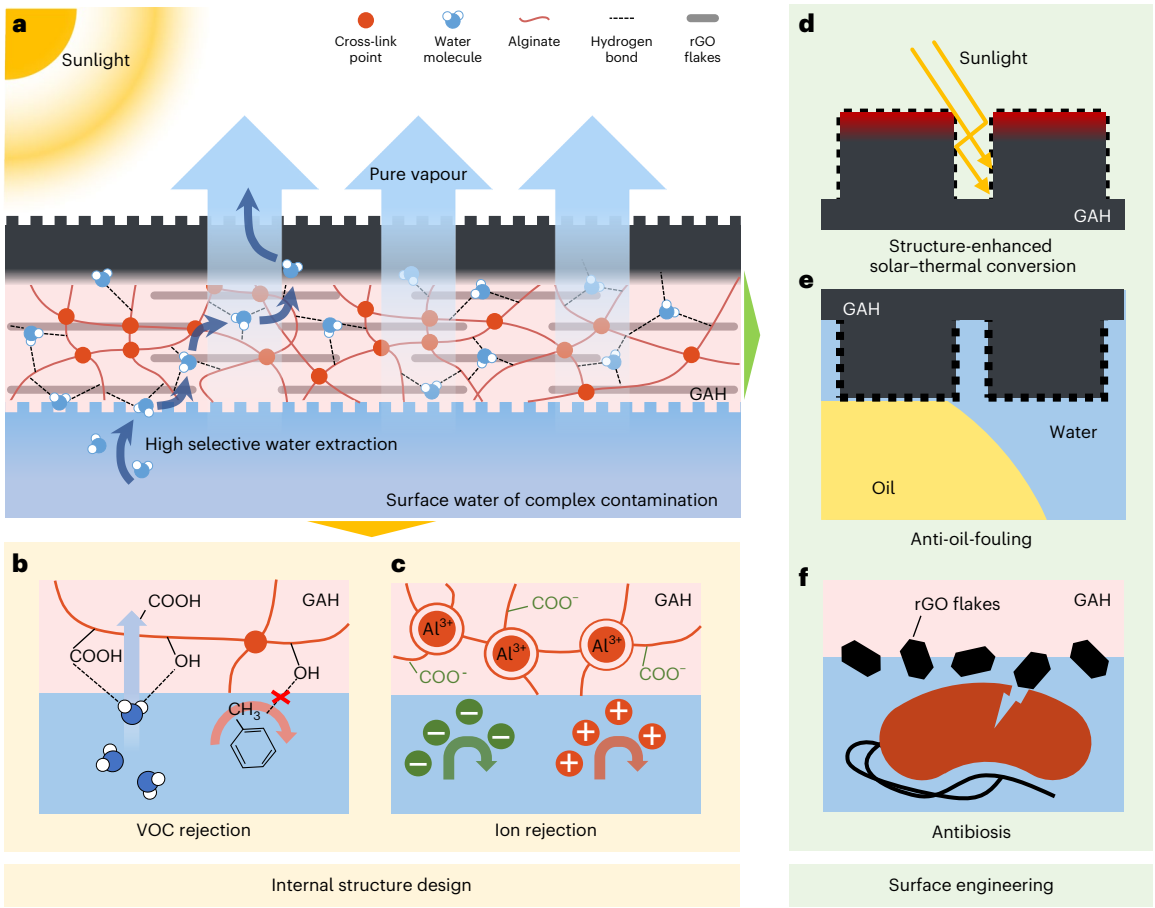

Fig. 1 | Schematic explanation of merits of GAH in clean water production. **a**, High selectivity of GAH in solar-powered pure water extraction and multi-effective antifouling capacity against surface water of complex contaminants. **b**, Different molecular interactions of water and contaminant molecules with GAH for selective water absorption and rejection of VOCs. **c**, Ion rejection based on a large difference in osmotic pressure between GAH and contaminated surface water. **d**, Efficient solar–thermal conversion based on fish-scale-inspired micro–nano-structured surface. **e**, Anti-oil-fouling effect due to underwater oleophobicity that is induced by a fish-scale-inspired micro–nano-structured surface of GAH. **f**, Antibiosis function due to exposed rGO sheets on the surface of GAH.

solar-powered interfacial materials into produced water[22], which are harmful and toxic even at a very low concentration[2]. Non-volatile organic compounds (NOCs) are often in the form of water-insoluble oil that can block the pores of solar-powered interfacial materials and limit water transmission[23–25]. A large number of bacteria present in surface water can adhere to the surface of solar-powered interfacial materials and render them ineffective[26,27]. All these will result in a dramatic loss of productivity in solar-powered clean water in real applications.

In this Article, a graphene/alginate hydrogel (GAH) is developed in combination with a hyper-dense internal structure design and bio-inspired surface engineering. It demonstrates high selectivity in solar-powered pure water extraction and multi-effective antifouling capacity against surface water containing complex contaminations (Fig. 1a). The high selective water transport against VOCs stems from absence of bulk water, and the different abilities of water and contaminant molecules to transport in bound state by forming enough hydrogen bonds with the polymer network in GAH (Fig. 1a,b). Rejection of ions is achieved by building up a high difference in osmotic pressure between GAH and contaminated surface water (Fig. 1c). With a fish-scale-inspired graphene-contained micro–nano-structured surface, the solar–thermal conversion capacity is enhanced by structure trapping of incident light (Fig. 1d), the underwater anti-oil-fouling function is achieved by super oleophobicity based on hydrophilic micro–nano structure-induced Cassie contact (Fig. 1e), and surface antibiosis is obtained from the exposed reduced graphene oxide (rGO) nanosheets (Fig. 1f). As a result, this GAH harvests clean water from contaminated surface water by rejecting >99.5% of VOCs, 99.3% of ions (Na^+, Mg^{2+}, K^+ and Ca^{2+}) and 100% of NOCs and bacteria. In addition, GAH has a submerged oil contact angle of >140° to carry oil-adhesion rejection, surface antimicrobial effect of nearly 100% and an ion rejection of 94.9% for seawater, leading to a desirable antifouling capacity in complex conditions that goes far beyond that in previous reports. Our study is of notable value for promoting the solar-powered clean water harvesting technology and addressing contaminated hydrological environments.

Results

Preparation and characterization of GAH

To prepare GAH, a dispersion of sodium alginate and graphene oxide was mixed and gelated at 40 °C and 50% relative humidity, followed by chemical reduction and multiple aluminium-ion-induced cross-linking cycles to form a dense rGO/alginate hydrogel (details are provided in Methods). Then, direct-laser writing was used to print the fish-scale-inspired micro–nano multi-scale pattern on the surfaces (Fig. 2a and Supplementary Figs. 1 and 2). As shown in Fig. 2b, the obtained GAH appears optically dark because of strong light absorption of rGO. In comparison, the alginate hydrogel without rGO is transparent (Supplementary Fig. 3). This GAH exhibits favourable mechanical flexibility that can be bent easily in any arbitrary curvature without fracture (Fig. 2b). The cross-section scanning electron microscopy (SEM) image exhibits a uniformly cross-linked densely packed laminar structure in GAH (Fig. 2c,d

https://doi.org/10.1038/s44221-023-00152-y

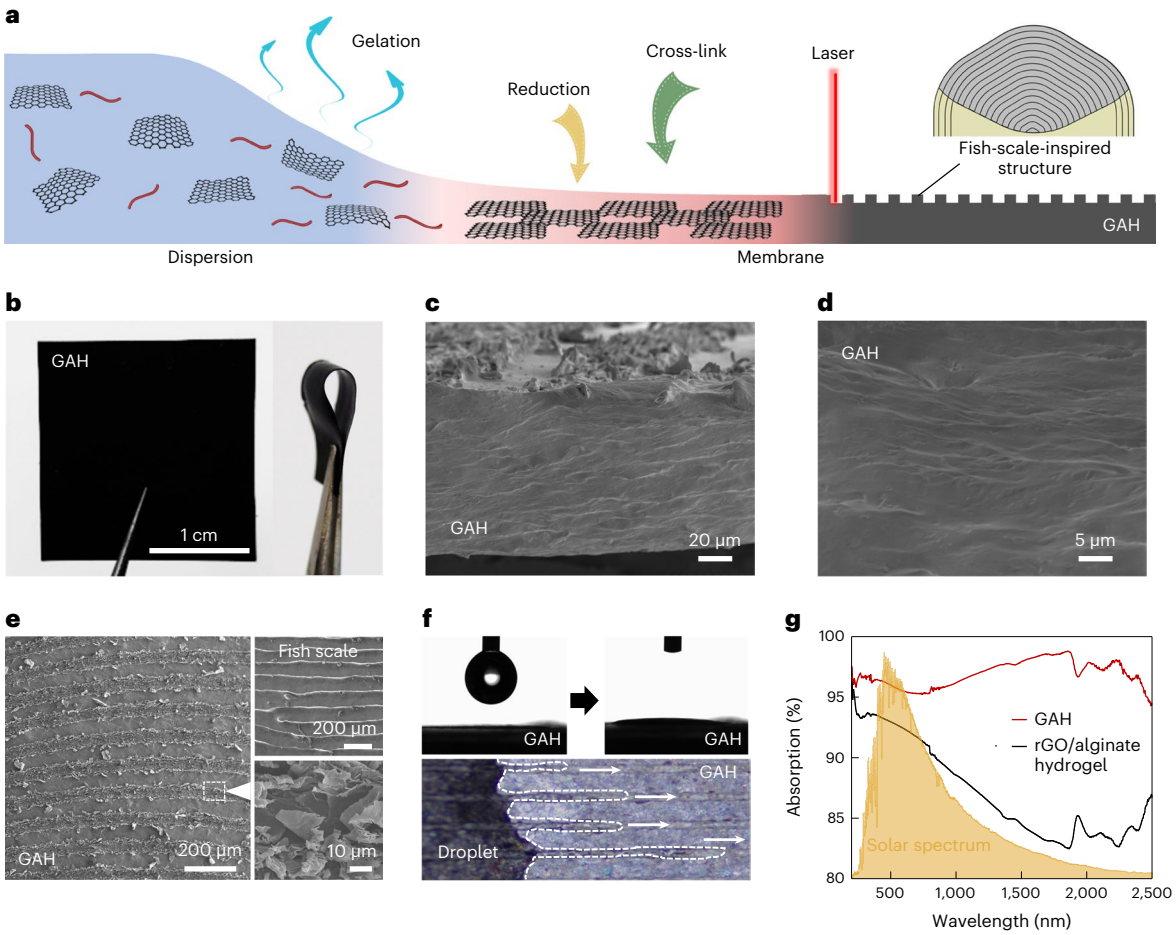

Fig. 2 | The fabrication and characterization of GAH. a, Schematic of the gelation, reduction, cross-linking and laser printing for the fabrication of GAH. **b**, Photographs of GAH membrane to show the black appearance (left) and flexibility (right). **c**, Cross-sectional SEM image of GAH. **d**, An enlarged view of **c**. **e**, SEM image of GAH surface and the real fish-scale surface. **f**, The images of water contact angle of GAH and the water droplet transport on the fish-scale-inspired surface of GAH (the white arrows describe the direction of droplet transmission). **g**, UV–Vis–near-infrared spectra of GAH (red curve), and rGO/alginate hydrogel without fish-scale-like pattern (black curve).

and Supplementary Fig. 4) without obvious seams, which will prevent transport of impurities inside by capillary bulk water (Fig. 2d), making it drastically different from most porous solar-powered water harvesters[27–38]. SEM image of the GAH surface shows uniform and striated microstructures with exposed rGO nanosheets (Fig. 2e). Micron stripes on the surface of GAH have an average width of 45 ± 10 μm and an interval of 100 ± 10 μm, similar to that of fish scale, with extra nanosheets packed along the stripes (Fig. 2e and Supplementary Fig. 1). This hierarchical micro–nano structure renders the GAH a superior hydrophilicity. As indicated in Fig. 2f, water droplets spread rapidly along the stripes on the surface and end up with a contact angle of 0° that is significantly lower than 10° of rGO/alginate hydrogel membrane without the fish-scale-like pattern[39]. Meanwhile, an absorbance of 95% within the full spectrum of sunlight is achieved by GAH because of multiple reflection of the incident light within GAH for a maximum conversion into heat, which largely surpasses the pattern-free rGO/alginate hydrogel (Fig. 2g). As a result, the patterned surface and dense structure of GAH provides the material basis for high performance in selectivity and fouling rejection in clean water production.

Water state within GAH

Micro-porous membrane is commonly used in solar-powered water production (Fig. 3a), for fast bulk water transport driven by capillary force[35]. However, bulk water always carries contaminants such as VOCs to evaporation surface and causes impurity of vapour[36]. Bulk water will be avoided, and all water molecules are mainly hydrogen bonded to polymer chains (Fig. 3b) in GAH illustrated as follows. The rGO/alginate in GAH is rich in oxygenate functional groups, providing abundant sites for multiple cross-linking cycles. Each cycle consists of ionic cross-linking by $AlCl_3$, stressing and drying. These GAHs are termed GAH-x, where x denotes the number of cross-linking cycles. The saturated water content (C_w) in GAH is first tested, which is defined as follows[22].

$$C_w = (Q_s - Q_d)/Q_d$$

where Q_s is the mass of saturated GAH and Q_d is the mass of the GAH after drying at 50 °C for 10 h. As shown in Fig. 3c, C_w decreases from 61.3% (GAH-1) to 13.1% (GAH-4), which indicates densification of the inner structure. As x increases, the tensile strength of GAH-x is also enhanced (Supplementary Fig. 5). The phase change behaviour of water is then monitored to study internal water state. GAH in a saturated state was completely solidified at −70 °C and gradually warmed up to 30 °C still in a solid state. As determined by differential scanning calorimetry (DSC) in Fig. 3d, GAH-1 has an endothermic peak near 0 °C, indicating the presence of bulk water, a state that can carry pollutants easily in the transport process[22]. This peak in GAH-2 was shrunk and shifted to the left, that is, less water in a bulk state and more water distributed in the inner rGO/alginate networks via hydrogen bonding interactions. The DSC curves of GAH-3 and GAH-4 present no obvious peaks, suggesting the absence of water in a bulk state. Meanwhile, the average

https://doi.org/10.1038/s44221-023-00152-y

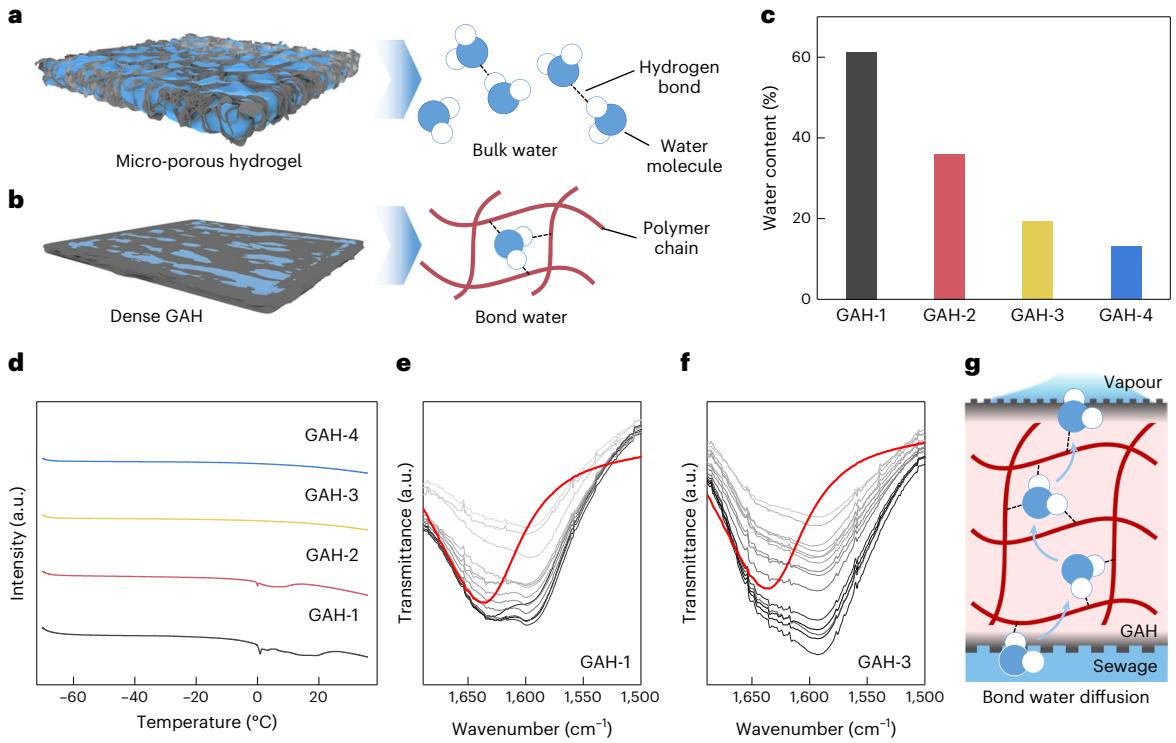

Fig. 3 | Bound water state in GAH-3. a, Scheme of water-saturated micro-porous materials and induced bulk water inside. **b**, Scheme of water-saturated GAH and induced bound water with polymer chains. **c**, Saturated water content of GAH-*x*. **d**, Heat flow of water-saturated GAH-*x* from −70 °C to 30 °C, analysed by DSC. **e**, FTIR spectra of pure water (red curve) and GAH-1 (black curves). **f**, FTIR spectra of pure water (red curve) and GAH-3 (black curves). The brightness gradient of black curves represents GAH-1 and GAH-3 of different water contents from saturated state (dark) to air-dried state (light). **g**, Scheme of bound water diffusion in GAH.

number of hydrogen bonds formed between each water molecule and the polymer chains in water-saturated GAH-*x* (termed as $N_{HB\text{-}x}$) can be calculated to indicate the water state in GAH-*x* (detailed information in Methods). As indicated (Supplementary Table 1), each water molecule in water-saturated GAH-1 could have about 0.84 hydrogen bonds with the polymer chains, suggesting some water molecules inside GAH-1 could be at the bulk water state[40]. The calculated $N_{HB\text{-}3}$ of GAH-3 is about 2.67 and $N_{HB\text{-}4}$ of GAH-4 is about 3.92, which means water molecules inside GAH-3 and GAH-4 are bonded with polymer chains, which is very different from that bulk state in GAH-1. In addition, Fourier transform infrared spectrometer (FTIR) tests are conducted to confirm the difference of water states in GAH-*x*. The hydroxyl bending mode absorption near 1,600 cm^{-1} is a powerful reporter for the hydrogen bonding state of water molecule[38]. As shown in Fig. 3e,f, the red curve represents the infrared absorption of pure water corresponding with hydroxyl bending mode absorption peak at 1,637 cm^{-1}, indicating bulk state of water molecules. The hydroxyl bending mode absorption of water-saturated GAH-1 is wide and has two small peaks (1,630 cm^{-1} and 1,598 cm^{-1}, Fig. 3e). With the decrease of water content in GAH-1, the relative intensity of these two peaks (1,630 cm^{-1} and 1,598 cm^{-1}) undergoes a significant change. And when water content becomes to be about 15%, the relative intensity of these two peaks (1,630 cm^{-1} and 1,598 cm^{-1}) is stable, indicating that there would remain water molecules of bound state with polymer chains in GAH-1 after some water evaporation. In other words, there would be at least two types of water molecule (bulk water state and bound state) in GAH-1 at the water-saturated state. However, for GAH-3, the relative intensity of these two peaks (1,630 cm^{-1} and 1,598 cm^{-1}) is always stable from the initial water-saturated state to final low water content state (Fig. 3f), reflecting water absorbed in GAH-3 is mainly at the bound state with polymer chains[41].

Based on these results, because there are not obvious penetrating micro/nano channels within GAH-3, the water transport across GAH-3 could be different from the micro/nano channel capillary force-induced bulk water transport process. Water molecules should be changed into the bound state with polymer chains through hydrogen bonds first, and then diffuse to the other side through the formed hydrogen bonds only (Fig. 3g), which avoids bulk water transport-induced pollutants passing through[36]. Meanwhile, it is difficult for most contaminant molecules to form sufficient hydrogen bonds with the polymer chains and enter GAH-3 due to the weaker dipole–dipole interaction between most contaminants and GAH[42]. Even after soaking GAH-3 in analytical reagents 1,4-dioxane, benzene and methylbenzene for 20 min, FTIR results of soaked GAH-3 demonstrate there are not significant representative peaks of these contaminant solvents, confirming the selective absorption capacity of water molecules (Supplementary Fig. 6). Hence, selective bound water absorption and diffusion will be achieved. To retain adequate water transport capability (Supplementary Fig. 7), GAH-3 rather than GAH-4 is employed for the following solar-powered freshwater extraction tests.

Selective solar-powered water extraction

GAH extracts pure water from sewage at both high efficiency and selectivity in practice. Because of the fish-scale-inspired surface structure, sunlight will be highly absorbed and turned into heat on the GAH for faster solar-powered water harvesting. The surface temperature of GAH can reach as high as 80 °C under one sun (1 kW m^{-2}) irradiation[43–45]. This capability of efficient solar–thermal conversion helps GAH extract pure water from sewage selectively[46]. The vapour is rapidly generated at a measured rate of 1.45 kg m^{-2} h^{-1} (1 kW m^{-2}), which is above eight times of bare water without GAH under the same conditions (0.18 kg m^{-2} h^{-1}, Fig. 4a). Extraction rate would be further increased

https://doi.org/10.1038/s44221-023-00152-y

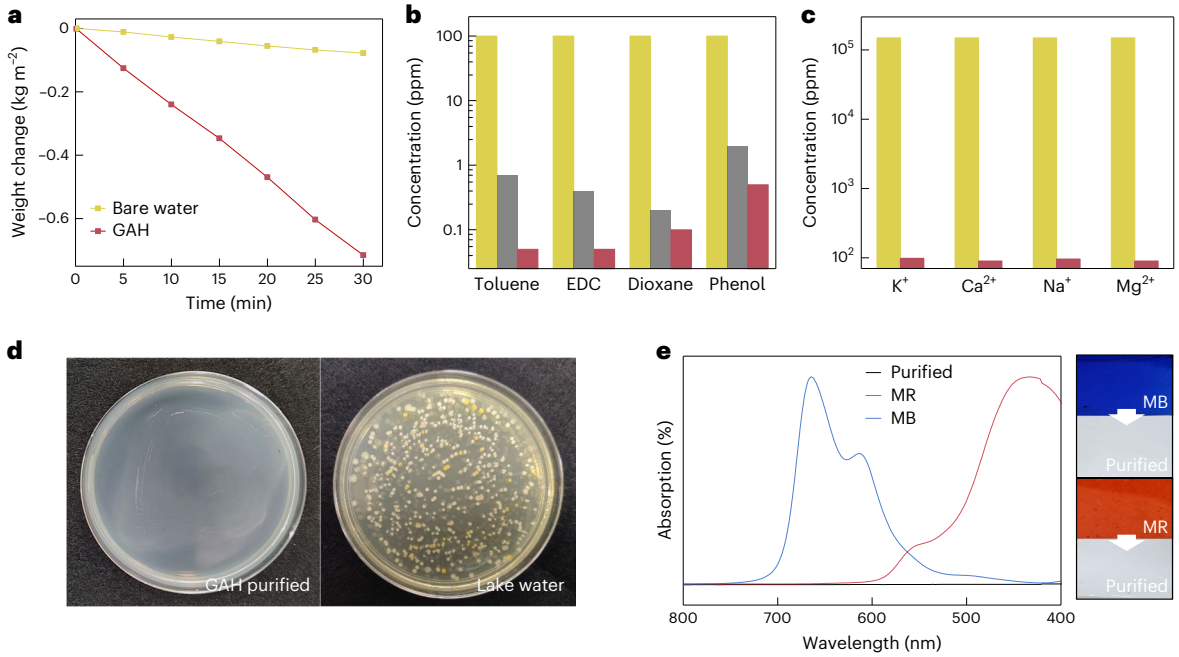

Fig. 4 | Performance of GAH in clean water selective harvesting. a, Vapour generation rate plots of GAH and bare water under one standard sunlight. **b**, Concentrations of toluene, dichloroethane (EDC), dioxane and phenol in raw sewage (yellow column) and GAH extracted water (red column). Grey column indicates drinking water standard adopted from World Health Organization or Environmental Protection Agency. **c**, K^+, Ca^{2+}, Na^+ and Mg^{2+} concentration in raw sewage (yellow column) and water extracted by GAH (red column). **d**, Images of culture dish growth with raw lake water (right) and GAH extracted water (left). **e**, UV–Vis absorption spectra of methyl red, methylene blue solution and GAH extracted water. Images at the right side show the colour of solution of red (methyl red, MR) and blue (methylene blue, MB) to colourless and transparent (GAH extracted water).

by a three-dimensional device design to 2.51 kg m^{-2} h^{-1}, and the efficiency is evaluated as ~82.6% (Supplementary Fig. 8). To verify the purity of extracted water, a home-made system is designed to harvest the water in a sealed container (Supplementary Fig. 9). As shown in Fig. 4b, three typical VOCs (toluene, dichloroethane and dioxane) in the raw sewage are at a level of 100 ppm, while in the extracted water, they drop below 0.07 ppm, pointing to a VOC removal efficiency of 99.93%. This effect should be caused by the selective bound water absorption with polymer chains in GAH and the weaker dipole–dipole interactions in VOCs–GAH than the H-bond interaction in water–GAH, which facilitates transport of water more than VOCs[22]. Meanwhile, GAH has rejection rates of >99.5% for phenol, since the phenolic hydroxyl groups form weaker H-bonds with inner rGO/alginate networks than water[47,48]. The high removal efficiency of VOCs by GAH in the solar water extraction is superior to those in many previous reports (Supplementary Fig. 10). In addition, K^+, Ca^{2+}, Na^+ and Mg^{2+} are examined in the extracted water. The solution with each ion concentration of 1.5 wt.% was employed as the raw sewage to be purified. As shown in Fig. 4c, the concentrations of ions (K^+, Ca^{2+}, Na^+ and Mg^{2+}) are below 100 ppm in extracted water, indicating ion rejection >99.3%. To verify GAH's power to produce bacteria-free water, raw water from domestic river and water extracted by GAH were taken for the bacteria regrowth test. The samples were incubated in a medium at 37 °C for 48 h. While no bacterial colony was found in the medium of extracted water shown, a large number of colonies were identified for the case of river water, supporting a nearly 100% efficiency for removing bacteria by GAH (Fig. 4d). Finally, methyl red, methylene blue and several other kinds of pigment are taken as representatives of NOC tests. As shown in the ultraviolet–visible (UV–Vis) spectra in Fig. 4e, the characteristic peaks of these NOCs are clearly seen in the polluted water at a concentration level of 15 ppm. In comparison, there are no signals of pigments in the solar-powered extracted water by GAH. Meanwhile, the colour of water turns from red (methyl red solution) or blue (methylene blue) into transparent (GAH extracted water) (Fig. 4e). Aqueous solutions of various pigments and their mixtures are further measured. The extracted water by GAH is clear and has no obvious signals of the mixed pigments (Supplementary Fig. 11). All these results verify the remarkable capability of GAH in solar-powered selective water harvesting by rejecting multiple complex pollutants.

Antifouling of GAH against oil, bacteria and salts

The antifouling function of GAH against oil, bacteria and salt adhesion is important for practical applications. As shown in Fig. 5a, GAH achieves a contact angle of 143° with soybean oil underwater, and the oil droplets remain largely spherical and do not adhere on the GAH. This is because the hydrophilic micro–nano structure traps water in the rough surface, forming a stable Cassie contact with oil drips underwater (Fig. 5b and Supplementary Fig. 12). Accordingly, GAH exhibits contact angles greater than 140° with common oily organic solvents (toluene, hexane, benzene, petroleum ether and cyclohexane) (Fig. 5c), showing excellent anti-oil-fouling property. This performance is similar to the interaction between fish scales and oil (Supplementary Fig. 13), indicating that micro–nano structure induces favourable oil stain prevention. Meanwhile, two-dimensional rGO nanosheets are widely reported to have bacterial toxicity because of chemical sterilization of oxygen-containing functional groups and physical sterilization of nano-defects and edges[49,50]. The fish-scale-inspired micro–nano surface of GAH is rich in rGO nanosheets, ensuring the inheritance of the antibiosis behaviour of rGO (Fig. 5d). To verify this, the number of bacteria in raw sewage before and after contacting with GAH is compared. Domestic river water is taken as the raw sewage containing multiple kinds of bacteria. In the experimental group, the raw sewage was applied on the surface of GAH before regrowth, and the system error was ruled out with a control group identically treated without GAH. As shown in Fig. 5e, as the number of bacteria in raw sewage group is defined as 100%, 78% of bacteria survived on the samples in the control group, but less than 1%

https://doi.org/10.1038/s44221-023-00152-y

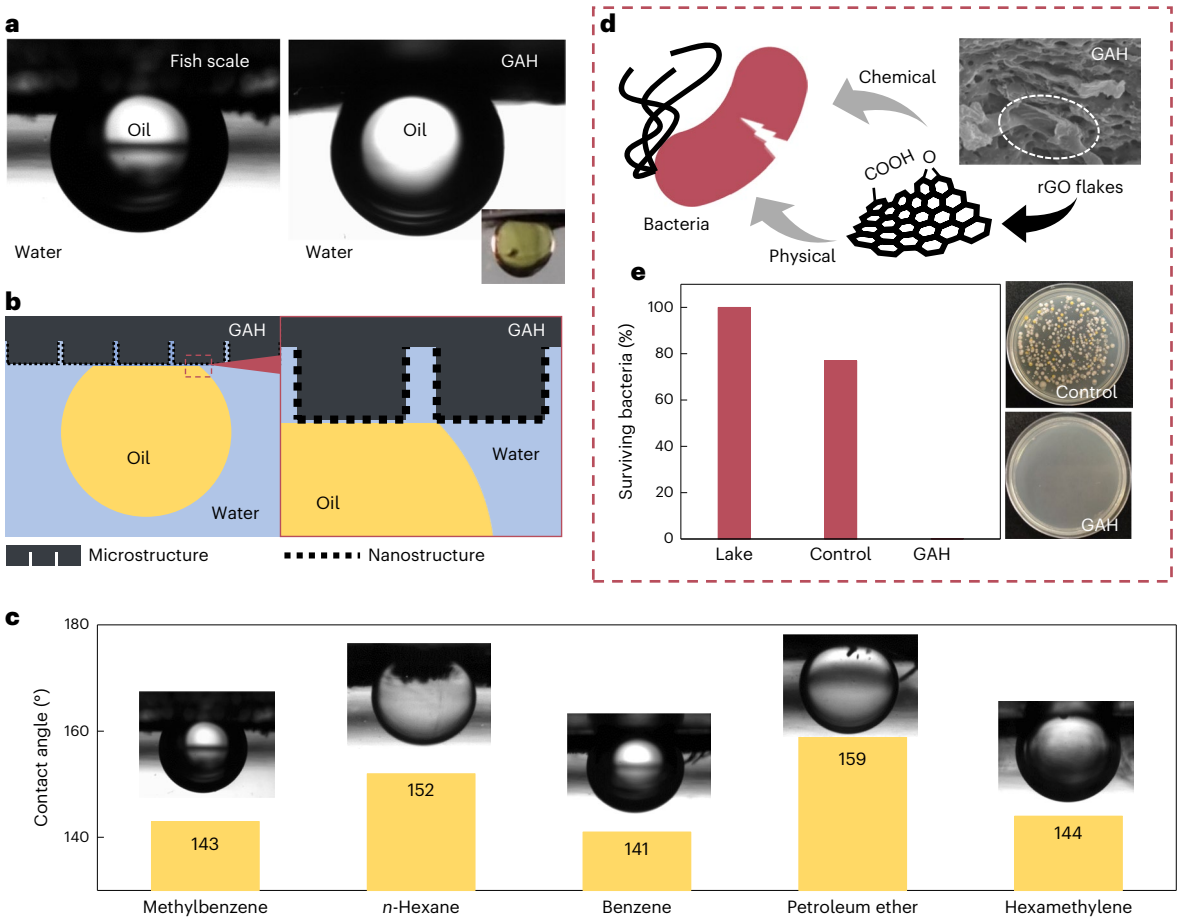

Fig. 5 | Super antifouling performance of GAH in polluted raw sewage. **a**, Images of oil contact angle in water formed by fish scale (left) and GAH (right). Inset is the image of soybean oil on GAH. **b**, Mechanism of GAH's anti-oil-fouling capacity by forming a stable solid/water/oil system on the patterned surface. **c**, Contact angle of methylbenzene, *n*-hexane, benzene, petroleum ether and hexamethylene on GAH surface under water. **d**, Mechanism of antibiosis of GAH based on rGO sheets on its patterned surface. Chemical sterilization of oxygen-containing functional groups and physical sterilization of nano-defects and edges contributes to antibiosis capacity. **e**, Regrowth test result of diluted raw lake water, control group and GAH-treated group. Images on the right refer to the culture dishes of control group and GAH-treated group.

survived on samples in the GAH-treated experimental group. SEM image shows the broken pieces of dead bacteria (Supplementary Fig. 14).

Salt fouling on the solar-powered water harvester is a serious problem. As vapour is generated, ions in sewage will become concentrated, crystallize and accumulate to cause salt fouling[51,52]. Because of rich anions (for example, -COO^-) and cations (Na^+ and Al^{3+}) produced by ionization in rGO/SA network, densified by multiple cross-linking cycles, GAH is extremely dense in ions, forming a large osmotic pressure to pump water into GAH while repelling ions in sewage (Fig. 6a)[17]. To verify this, GAH was put into NaCl solutions of different concentrations to be saturated. By comparing NaCl concentration in NaCl solution and the absorbed NaCl concentration by GAH at equilibrium state, the ion rejection rate (REJ) of GAH can be calculated (detailed information in Methods and Supplementary Fig. 15). Figure 6b shows REJ of GAH in NaCl solution of different concentrations. When the NaCl concentration is 3.6 wt.%, REJ reaches as high as ~94.9%. Even when NaCl concentration is close to the saturation (25 wt.%), GAH maintains an REJ of about 24%. The osmotic pressure of saturated NaCl solution can be calculated by the formula $\pi = iCRT$ (where i is the dimensionless van't Hoff index, which is 2 for NaCl, R is the ideal gas constant and T is the Kelvin temperature), which is about 280 atm. GAH still demonstrates a high REJ ability in the saturated NaCl solution mentioned above, which means GAH should have much higher osmotic pressure than that of saturated NaCl solution (~280 atm), preventing the entry of ions from the tested solution even under saturated state.

To clarify the practical salt fouling preventing performance, GAH was tested for 5 days. Artificial sunlight of 750 W m^{-2} was used for GAH to extract clean water from seawater (Fig. 6c), and 12-h light irradiation time was used to simulate the daytime in 1 day (24 h). During the first day, W_{in} reaches only 0.25 wt.% after 12-h light exposure caused by high REJ, which is much lower than the solubility of NaCl (26.4 wt.%, room temperature), excluding risk of salt fouling, while after 12-h dark time, W_{in} decreases to 0.18 wt.% because of outward ion migration from GAH to surrounding solution driven by osmotic difference (Fig. 6d). This outward ion migration refreshed W_{in} before light exposure, preventing cross-day ion accumulation in GAH. During the 5-day test, the daily W_{in} after 12-h dark time remained stable at around 0.18 wt.%, which means that ions accumulated in GAH during the daytime completely migrate into surrounding solution at night, ensuring stable W_{in} after 12-h light exposure around 0.25 wt.% (Supplementary Fig. 16). Based on this daily refreshment, GAH gains stable performance during long-term employment. The ion rejection capacity remained at about 99.8% of the initial value, and the water extraction rate and surface structure at the fifth day almost stayed unchanged (Fig. 6e). In addition, after 20 h of vapourizing under one standard sunlight, no salt-fouling appeared on GAH in 17 wt.% highly concentrated NaCl solution. All these results indicate excellent salt fouling prevention of GAH.

https://doi.org/10.1038/s44221-023-00152-y

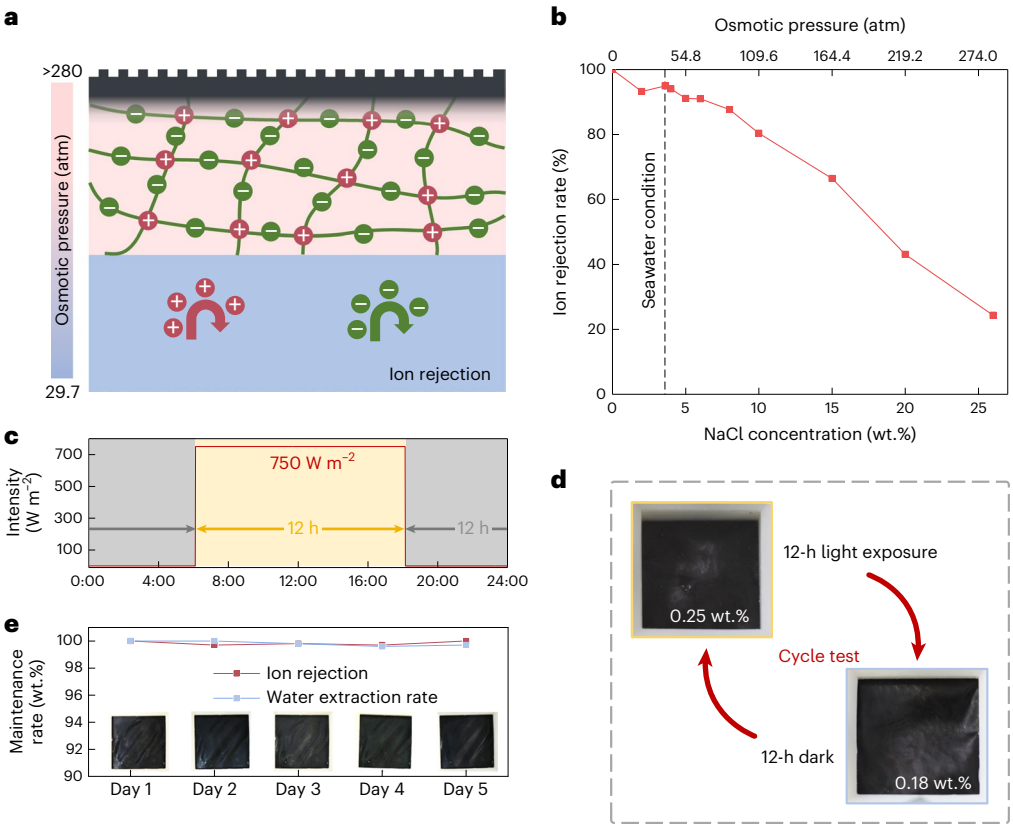

Fig. 6 | Ion rejection mechanism and practical performance of GAH. a, Ion rejection mechanism of GAH based on high osmotic pressure of hyper-dense and cross-linked rGO/alginate network. **b**, Calculated ion rejection rate of GAH-3 in NaCl solution of different concentrations. Upper lateral axis represents calculated osmotic pressure of NaCl solution. **c**, Lab-simulated solar condition in one 24-h day. **d**, Periodic light conditions of cycle tests with alternative 12-h light exposure and 12-h dark time. Photographs show the clean surface of GAH after 12-h light exposure and 12-h dark time. **e**, Maintenance rate of ion rejection and water extraction rate during the 5-day test. Inset images are the appearance of GAH (2 cm × 2 cm) for each day.

Conclusion

We successfully developed a solar-powered water extraction GAH system with high selective water transport and multifunctional super antifouling effect to directly harvest clean water from sewage containing complex contaminants. Assisted by fish-scale-inspired surface engineering and a hyper-dense internal rGO/alginate network, GAH carries several merits: (1) structure-enhanced high-efficiency solar–thermal conversion, absorbing >95% of sunlight to heat the surface to 80 °C under one standard sunlight; (2) high selective water transport based on inner bound water state and the different abilities to form hydrogen bond between water molecule–GAH and contaminant molecule–GAH, to reject more than 99.5% of VOCs; (3) oil-adhesion prevention by building stable Cassie contact underwater with hydrophilic micro–nanostructured surface, to form contact angle >140° with organic solvent; (4) antibiosis based on exposed rGO nanosheets to deactivate ~100% bacteria on surface; and (5) anti-salt-fouling by building up higher osmotic pressure of GAH than sewage, with charged group produced by ionization in hyper-dense rGO/SA network, rejecting 94.9% ions in seawater from entering, keeping ultralow internal salt concentration during 5-day test without fouling. The concept in developing GAH is of great importance for the practical application of low-carbon water purification strategies and contributing to solve the global drinking water crisis.

Methods

Preparation of GO suspension

GO suspension was prepared according to a modified Hummers method as reported previously[22,53,54]. First, 3 g natural graphite (325 mesh) and 70 mñ concentrated sulfuric acid (98 wt.%) were uniformly mixed and stirred at 0 °C for 30 min. Then, 9 g potassium permanganate was added to this mixture carefully in small amounts and several times. Next, the reaction mixture was transferred to a 40 °C water bath and stirred for 30 min. Then, 150 ml of de-ionized water was carefully added. The dispersion was stirred violently for 15 min, and the system temperature was kept at 90 °C by water bath. Next, an additional 500 ml de-ionized water was added, followed by the addition of 15 ml hydrogen peroxide (30 wt.%) until the solution became orange–brown. The resulting solution was filtered and washed with 200 ml hydrochloric acid (3.7 wt.%) for 12 h. The derived filter cake was dispersed in de-ionized water, and the obtained dispersion was stirred for 12 h. Any unexfoliated graphite was removed by centrifuging the solution at 3,000 rpm for 30 min with the precipitation discarded. Then, the dispersion was put into the dialysate bag (8,000–14,000 Da) and dialysed for a week to remove residual ions. The collected GO was concentrated by centrifugation and then diluted using de-ionized water.

Preparation of GAH

The GAH was prepared by sequential ionic cross-linking, reduction and direct-laser writing. Sodium alginate (Macklin, 5,000 mPa s^{-1}, 1% in water at 25 °C) was used to prepare 15 ml of 2 wt.% alginate solution in water. Then, 5 ml of 10 mg g^{-1} GO dispersion was added, and the mixture was stirred for 1 h. The solution was centrifuged at 1,475*g* for 20 min to remove the bubbles and sediment. The dispersion was next transferred into a glass container and dried at a temperature of 60 °C for 12 h to form a membrane. The obtained membrane was cross-linked for multiple cycles. During each cycle, the membrane was cross-linked

by soaking into a 0.5 M $AlCl_3$ aqueous solution for 12 h, then washed with de-ionized water and dried in oven. Cross-linked membrane was reduced at 70 °C for 10 h. After multiple cycles, the fish-scale-inspired micro–nano structure was written by HGTECH LSU3EA laser system (355 nm, 30 kHz). The laser power is 3 W, and the scanning speed is 1,000 mm s^{-1}.

Characterization

The structures and element mapping were characterized by SEM (FlexSEM 1000). FTIR spectra were collected by UATR Two FTIR spectrometer. Thermogravimetric analysis was performed by using a thermogravimetric analyser (TGA/DSC, STA449F3) under air, and the heating rate was 10 K min^{-1}. The temperature distribution was recorded using an infrared camera (Fluke TiX640) in real time. The ion concentrations of water were assessed using an inductively coupled plasma emission spectrometer (Vista-MPX). The optical transmittance and reflectance spectra of the aerogel were measured on a UV–Vis spectrophotometer (Cary 5000) with an Agilent integrating sphere. All weights were measured by analytical balance (Mettler Toledo ME104E).

Calculation of average number of hydrogen bonds formed between each water molecule and the polymer chains

Average number of hydrogen bonds formed between each water molecule and the polymer chains in water-saturated GAH-*x* is calculated by the following method, which would reflect the water molecule state inside[55].

$$N_{HB-x} = \frac{n(m_{GAH-x} - m_{Al} - m_g)/M_{unit}}{Q_w \times m_{GAH-x}/M_w}$$

where $N_{HB\text{-}x}$ is the average number of hydrogen bonds formed between each water molecule and the polymer chains; $m_{GAH\text{-}x}$, m_{Al} and m_g is the mass of water-saturated GAH-*x* sample, Al^{3+} and graphene, respectively; Q_w is the water content of water-saturated GAH-*x*; M_{unit} is the molar mass of alginate repeating unit (~198 g mol^{-1}); *n* is the active sites for hydrogen bonding provided by alginate repeating unit (four O-sites and two H-sites); and M_w is the molar mass of water molecule (18 g mol^{-1}).

Vapour extraction rate measurements and removal test

In this experiment, a lab-made device was designed (Supplementary Fig. 5) that is made of Teflon with a 2 cm × 2 cm evaporation window in the centre, to cover the membrane in order to control the light area. The membrane was in contact with water below to ensure water supply. While working under one standard sunlight generated by sunlight generator (91150V, Newport) for 0.5 h, the weight loss of the whole equipment was recorded every 5 min to calculate the vapour extraction rate. For VOC rejection test, aqueous solution with VOCs of 100 ppm was taken as the raw sewage. The VOC concentration of collected water was measured by Agilent Technologies gas chromatograph–mass spectrometer. For ion removal test, 1.5 wt.% of Na^+, Mg^{2+}, K^+ and Ca^{2+} solutions was prepared with chloride as anion. The ion concentration of collected water was measured with inductively coupled plasma mass spectrometer (iCAP Q, Thermo, Waltham). For NOC removal test, 10 mg ml^{-1} methylene blue and methylene red sodium solutions were prepared as raw sewage. The pigment concentration of collected water was measured by a UV–Vis spectrophotometer (DR/5000).

Bacteria removal test

Domestic river water was used as raw sewage for the bacteria source. Water condensed from the vapour generated by GAH was collected as purified sample. The river water and the GAH-purified water to be tested were diluted 10,000 times, and then 1 ml was evenly applied to the surface of the total nutrient medium, and the medium was placed at 37 °C for 48 h, after which the antibacterial effect was compared according to the number of colonies.

Underwater contact angle measurements

A transparent water tank was filled with water, the materials (GAH and fish scale) to be measured were applied on a flat substrate downward over the water surface and the air between the material and the water surface was evacuated. Then, 12 µl of oily liquid in water was dropped through a J-shaped needle to the surface of GAH. The contact angle was measured by OCA 15 Plus Contact Angle Meter (Eastern-Dataphy).

Antibiosis test

Domestic river water was taken as the bacteria source. One millilitre of river water was applied to GAH with a diameter of 50 mm. Then, GAH was treated with ultrasonic for 30 min to accelerate and enhance the physical interaction. Then, 10 ml buffered solution at one time was used to wash the bacteria of GAH three times, and the elute was diluted to 100 ml followed by 100-fold dilution. One millilitre of diluent was used for regrowth test to measure the number of bacteria. Also, the 10,000-fold diluent of raw river water and river water treated by ultrasound without GAH were regrowth-tested as a control test to eliminate systematic errors[49].

Calculation of ion rejection rate

The ion rejection rate of GAH can be calculated by the formula REJ = $(1 - W_{in}/W_s) \times 100\%$. W_s represents NaCl concentration in NaCl solution, and W_{in} represents NaCl concentration in the absorbed NaCl solution by GAH at equilibrium state. The NaCl concentration in the absorbed NaCl solution by GAH can be calculated by the following equations.

$$W_{in} = m_{ion}/m_{sol}$$

The mass of absorbed NaCl solution (m_{sol}) by GAH and the mass of the NaCl in the absorbed water (m_{ion}) by GAH is obtained with the following equations.

$$m_{sol} = m_s - m_o$$

$$m_{ion} = m_d - m_o$$

where m_o, m_s and m_d represent the mass of original GAH, saturated GAH in NaCl solution and GAH after being dried, respectively.

Reporting summary

Further information on research design is available in the Nature Portfolio Reporting Summary linked to this article.

Data availability

The data generated in this study are provided in the main text, Methods or Supplementary Information.

References

1. Topuz, F., Holtzl, T. & Szekely, G. Scavenging organic micropollutants from water with nanofibrous hypercrosslinked cyclodextrin membranes derived from green resources. *Chem. Eng. J.* **419**, 129443 (2021).
2. Sisto, R. et al. Direct and oxidative DNA damage in a group of painters exposed to VOCs: dose-response relationship. *Front. Public Health* **8**, 445 (2020).
3. Chaplin-Kramer, R. et al. Global modeling of nature's contributions to people. *Science* **366**, 255–258 (2019).
4. Oki, T. & Kanae, S. Global hydrological cycles and world water resources. *Science* **313**, 1068–1072 (2006).
5. Downing, J., Polasky, S., Olmstead, S. & Newbold, S. Protecting local water quality has global benefits. *Nat. Commun.* **12**, 2709 (2021).
6. Al-Karaghouli, A. & Kazmerski, L. L. Energy consumption and water production cost of conventional and renewable-energy-powered desalination processes. *Renew. Sustain. Energy Rev.* **24**, 343–356 (2013).

7. Chitrao, P. V., Bhoyar, P. K., Chopra, K. & Divekar, R. Commercial viability of solar thermal hyper distillation of waste water—Sainnova, a case study. *Lect. Notes Netw. Syst.* **401**, 333–340 (2021).
8. Jones, E., Qadir, M., van Vliet, M. T. H., Smakhtin, V. & Kang, S. M. The state of desalination and brine production: a global outlook. *Sci. Total Environ.* **657**, 1343–1356 (2019).
9. Khawaji, A. D., Kutubkhanah, I. K. & Wie, J. M. Advances in seawater desalination technologies. *Desalination* **221**, 47–69 (2008).
10. Wei, Z., Wang, J., Guo, S. & Tan, S. C. Towards highly salt-rejecting solar interfacial evaporation: photothermal materials selection, structural designs, and energy management. *Nano Res. Energy* **1**, e9120014 (2022).
11. Zhang, M. & Yuan, J. Graphene meta-aerogels: when sculpture aesthetic meets 1D/2D composite materials. *Nano Res. Energy* **1**, e9120035 (2022).
12. Liang, H. X. et al. Thermal efficiency of solar steam generation approaching 100% through capillary water transport. *Angew. Chem. Int. Ed.* **58**, 19041–19046 (2019).
13. Yang, H. S. et al. Superplastic air-dryable graphene hydrogels for wet-press assembly of ultrastrong superelastic aerogels with infinite macroscale. *Adv. Funct. Mater.* **29**, 1901917.1–1901917.9 (2019).
14. Yao, H. Z. et al. Janus-interface engineering boosting solar steam towards high-efficiency water collection. *Energy Environ. Sci.* **14**, 5330–5338 (2021).
15. Li, Y. et al. Reborn three-dimensional graphene with ultrahigh volumetric desalination capacity. *Adv. Mater.* **33**, 2105853 (2021).
16. Zhang, P. P. et al. Direct solar steam generation system for clean water production. *Energy Storage Mater.* **18**, 429–446 (2018).
17. Zeng, J., Wang, Q., Shi, Y., Liu, P. & Chen, R. Osmotic pumping and salt rejection by polyelectrolyte hydrogel for continuous solar desalination. *Adv. Energy Mater.* **9**, 1900552 (2019).
18. Zhang, P. P., Li, J., Lv, L. X., Zhao, Y. & Qu, L. T. Vertically aligned graphene sheets membrane for highly efficient solar thermal generation of clean water. *ACS Nano* **11**, 5087–5093 (2017).
19. Alsaid, Y. et al. Tunable sponge-like hierarchically porous hydrogels with simultaneously enhanced diffusivity and mechanical properties. *Adv. Mater.* **33**, 2008235 (2021).
20. Zuo, P. et al. Shape-controllable gold nanoparticle–MoS_2 hybrids prepared by tuning edge-active sites and surface structures of MoS_2 via temporally shaped femtosecond pulses. *ACS Appl. Mater. Interfaces* **9**, 7447–7455 (2017).
21. Cui, L. F. et al. High rate production of clean water based on the combined photo-electro-thermal effect of graphene zrchitecture. *Adv. Mater.* **30**, 1706805 (2018).
22. Zhang, P. P. et al. Super water-extracting gels for solar-powered volatile organic compounds management in the hydrological cycle. *Adv. Mater.* **34**, 2110548 (2022).
23. Lu, H. Y. et al. High-yield and low-cost solar water purification via hydrogel-based membrane distillation. *Adv. Funct. Mater.* **31**, 2101036 (2021).
24. Lu, X. L. et al. Tuning the permselectivity of polymeric desalination membranes via control of polymer crystallite size. *Nat. Commun.* **10**, 2347 (2019).
25. Zou, Y. et al. A mussel-inspired polydopamine-filled cellulose aerogel for solar-enabled water remediation. *ACS Appl. Mater. Interfaces* **13**, 7617–7624 (2021).
26. Li, Y. et al. Composite hydrogel-based photothermal self-pumping system with salt and bacteria resistance for super-efficient solar-powered water evaporation. *Desalination* **515**, 115192 (2021).
27. Han, J. et al. Degradable GO-nanocomposite hydrogels with synergistic photothermal and antibacterial response. *Polymer* **230**, 124018 (2021).
28. Yang, W. et al. Natural flexible dermal armor. *Adv. Mater.* **25**, 31–48 (2013).
29. Chen, Q., Zhao, J., Cheng, H. H. & Qu, L. T. Progress in 3D-graphene assemblies preparation for solar-thermal steam generation and water treatment. *Acta Phys. Chim. Sin.* **38**, 2101020 (2022).
30. Yu, Z. et al. Enhanced interfacial solar evaporation through formation of micro-meniscuses and microdroplets to reduce evaporation enthalpy. *Adv. Funct. Mater.* **32**, 2108586 (2022).
31. Zhu, Y. Q. et al. Low-cost, unsinkable, and highly efficient solar evaporators based on coating MWCNTs on nonwovens with unidirectional water-transfer. *Adv. Sci.* **8**, 210727 (2021).
32. Li, Z. W. & Knetsch, M. Antibacterial strategies for wound dressing: preventing infection and stimulating healing. *Curr. Pharm. Des.* **24**, 936–951 (2018).
33. Ali, N. H., Amin, M. C. I. M. & Ng, S. F. Sodium carboxymethyl cellulose hydrogels containing reduced graphene oxide (rGO) as a functional antibiofilm wound dressing. *J. Biomater. Sci. Polym. Ed.* **30**, 629–645 (2019).
34. Wang, X. P. et al. A facile one-pot method to two kinds of graphene oxide-based hydrogels with broad-spectrum antimicrobial properties. *Chem. Eng. J.* **260**, 331–337 (2015).
35. Zhao, F. et al. Highly efficient solar vapour generation via hierarchically nanostructured gels. *Nat. Nanotechnol.* **13**, 489–495 (2018).
36. Simonich, S. L. & Hites, R. A. Global distribution of persistent organochlorine compounds. *Science* **269**, 1851–1854 (1995).
37. Hou, L. & Wu, P. Y. Exploring the hydrogen-bond structures in sodium alginate through two-dimensional correlation infrared spectroscopy. *Carbohydrate Polym.* **205**, 420–426 (2019).
38. Seki, T. et al. The bending mode of water: a powerful probe for hydrogen bond structure of aqueous systems. *J. Phys. Chem. Lett.* **19**, 8459–8469 (2020).
39. Liu, M. J., Wang, S. T., Wei, Z. X., Song, Y. L. & Jiang, L. Bioinspired design of a superoleophobic and low adhesive water/solid interface. *Adv. Mater.* **21**, 665–669 (2009).
40. Zhao, F., Guo, Y., Zhou, X., Shi, W. & Yu, G. H. Materials for solar-powered water evaporation. *Nat. Rev. Mater.* **5**, 388–401 (2020).
41. Liu, X., Liu, J., Lin, S. & Zhao, X. Hydrogel machines. *Mater. Today* **36**, 102–124 (2020).
42. Zhang, Y., Li, Y. & Liu, W. Dipole–dipole and H-bonding interactions significantly enhance the multifaceted mechanical properties of thermoresponsive shape memory hydrogels. *Adv. Funct. Mater.* **25**, 471–480 (2015).
43. Wu, L. et al. Highly efficient three-dimensional solar evaporator for high salinity desalination by localized crystallization. *Nat. Commun.* **11**, 521 (2020).
44. Chen, C., Kuang, Y. & Hu, L. Challenges and opportunities for solar evaporation. *Joule* **3**, 683–718 (2019).
45. Gao, M. M., Zhu, L. L., Peh, C. K. & Ho, G. W. Solar absorber material and system designs for photothermal water vaporization towards clean water and energy production. *Energy Environ. Sci.* **12**, 841–864 (2019).
46. Zhu, L. L., Gao, M. M., Peh, C. K. N. & Ho, G. W. Recent progress in solar-driven interfacial water evaporation: advanced designs and applications. *Nano Energy* **57**, 507–518 (2019).
47. Meunier, B. Catalytic degradation of chlorinated phenols. *Science* **296**, 270–271 (2002).
48. Xie, W. J. et al. Electrocatalytic activity of Pd-loaded Ti/TiO_2 nanotubes cathode for TCE reduction in groundwater. *Water Res.* **47**, 3573–3582 (2013).
49. Omid, A. & Elham, G. Toxicity of graphene and graphene oxide nanowalls against bacteria. *ACS Nano* **10**, 5731–5736 (2010).
50. Papi, M. et al. Biomimetic antimicrobial cloak by graphene-oxide agar hydrogel. *Sci. Rep.* **7**, 12 (2016).

51. Wang, C. B. et al. Superhydrophilic porous carbon foam as a self-desalting monolithic solar steam generation device with high energy efficiency. *J. Mater. Chem. A* **8**, 9528–9535 (2020).
52. Dong, X. Y. et al. Janus fibrous mats based suspended type evaporator for salt resistant solar desalination and salt recovery. *Small* **18**, 2107156 (2022).
53. Wu, W. P. et al. A versatile, heat-resisting, electrocatalytic active graphene framework by in-situ formation of boron nitride quantum dots. *Carbon* **192**, 123–132 (2022).
54. Yang, C. et al. A machine-learning-enhanced simultaneous and multimodal sensor based on moist-electric powered graphene oxide. *Adv. Mater.* **34**, 2205249 (2022).
55. Li, W. B., Xue, F. & Cheng, R. S. States of water in partially swollen poly(vinyl alcohol) hydrogels. *Polymer* **46**, 12026–12031 (2005).

Acknowledgements

This work was supported by the financial support from the National Science Foundation of China (nos. 22035005, 52022051, 22075165, 52090032 and 52073159) and Tsinghua-Foshan Innovation Special Fund (2020THFS0501). J.Y. thanks the Wallenberg Initiative Materials Science for Sustainability (WISE) funded by the Knut and Alice Wallenberg Foundation (project 197 under WISE-ap1 call).

Author contributions

L.Q., J.Y., H.C. and X.H. designed the experiments and accomplished the draft. H.Y., P.Z., Q.L. and K.Z. gave advice on experiments. J.Y. and J.C. contributed to data analysis and reviewed the manuscript. L.Q. supervised the entire project.

Funding

Open access funding provided by Stockholm University.

Competing interests

The authors declare no competing interests.

Additional information

Supplementary information The online version contains supplementary material available at https://doi.org/10.1038/s44221-023-00152-y.

Correspondence and requests for materials should be addressed to Huhu Cheng, Jiayin Yuan or Liangti Qu.

Peer review information *Nature Water* thanks Qunfeng Cheng and the other, anonymous, reviewers for their contribution to the peer review of this work.

nature portfolio

Corresponding author(s): Liangti Qu

Last updated by author(s): Sep 29, 2023

Reporting Summary

Nature Portfolio wishes to improve the reproducibility of the work that we publish. This form provides structure for consistency and transparency in reporting. For further information on Nature Portfolio policies, see our Editorial Policies and the Editorial Policy Checklist.

Statistics

For all statistical analyses, confirm that the following items are present in the figure legend, table legend, main text, or Methods section.

n/a	Confirmed	
☐	☒	The exact sample size (*n*) for each experimental group/condition, given as a discrete number and unit of measurement
☐	☒	A statement on whether measurements were taken from distinct samples or whether the same sample was measured repeatedly
☐	☒	The statistical test(s) used AND whether they are one- or two-sided *Only common tests should be described solely by name; describe more complex techniques in the Methods section.*
☐	☒	A description of all covariates tested
☐	☒	A description of any assumptions or corrections, such as tests of normality and adjustment for multiple comparisons
☐	☒	A full description of the statistical parameters including central tendency (e.g. means) or other basic estimates (e.g. regression coefficient) AND variation (e.g. standard deviation) or associated estimates of uncertainty (e.g. confidence intervals)
☐	☒	For null hypothesis testing, the test statistic (e.g. *F*, *t*, *r*) with confidence intervals, effect sizes, degrees of freedom and *P* value noted *Give P values as exact values whenever suitable.*
☐	☒	For Bayesian analysis, information on the choice of priors and Markov chain Monte Carlo settings
☐	☒	For hierarchical and complex designs, identification of the appropriate level for tests and full reporting of outcomes
☐	☒	Estimates of effect sizes (e.g. Cohen's *d*, Pearson's *r*), indicating how they were calculated

Our web collection on statistics for biologists contains articles on many of the points above.

Software and code

Policy information about availability of computer code

Data collection	no software was used
Data analysis	no software was used

For manuscripts utilizing custom algorithms or software that are central to the research but not yet described in published literature, software must be made available to editors and reviewers. We strongly encourage code deposition in a community repository (e.g. GitHub). See the Nature Portfolio guidelines for submitting code & software for further information.

Data

Policy information about availability of data

All manuscripts must include a data availability statement. This statement should provide the following information, where applicable:

- Accession codes, unique identifiers, or web links for publicly available datasets
- A description of any restrictions on data availability
- For clinical datasets or third party data, please ensure that the statement adheres to our policy

All data supporting the findings of this study are available in the main text, Methods , Supplementary Information or source data file.

Human research participants

Policy information about studies involving human research participants and Sex and Gender in Research.

Reporting on sex and gender	Not involved.
Population characteristics	See above.
Recruitment	No recruitment.
Ethics oversight	Not involved.

Note that full information on the approval of the study protocol must also be provided in the manuscript.

Field-specific reporting

Please select the one below that is the best fit for your research. If you are not sure, read the appropriate sections before making your selection.

☐ Life sciences ☐ Behavioural & social sciences ☒ Ecological, evolutionary & environmental sciences

For a reference copy of the document with all sections, see nature.com/documents/nr-reporting-summary-flat.pdf

Ecological, evolutionary & environmental sciences study design

All studies must disclose on these points even when the disclosure is negative.

Study description	We designed and prepared graphene/alginate hydrogel to characterize its basic properties and its effectiveness in the removal and antifouling of various contaminants.
Research sample	Graphene/alginate hydrogels with different number of cross-linking cycles, with and without fish-scale-inspired structures, which are prepared in lab.
Sampling strategy	Hydrogel samples were obtained from the same batch of prepared material to control system errors.
Data collection	All data is collected dy authors with the procedure stated in methods.
Timing and spatial scale	Comparison experiments were performed simultaneously in lab.
Data exclusions	No data were excluded from the analyses.
Reproducibility	All attempts to repeat the experiment is successful.
Randomization	Experiments were performed using randomized groups of prepared samples.
Blinding	There is no bias due to subjective judgment, and thus no need for blinding.

Did the study involve field work? ☐ Yes ☒ No

Reporting for specific materials, systems and methods

We require information from authors about some types of materials, experimental systems and methods used in many studies. Here, indicate whether each material, system or method listed is relevant to your study. If you are not sure if a list item applies to your research, read the appropriate section before selecting a response.

Materials & experimental systems

n/a	Involved in the study
☒	☐ Antibodies
☒	☐ Eukaryotic cell lines
☒	☐ Palaeontology and archaeology
☒	☐ Animals and other organisms
☒	☐ Clinical data
☒	☐ Dual use research of concern

Methods

n/a	Involved in the study
☒	☐ ChIP-seq
☒	☐ Flow cytometry
☒	☐ MRI-based neuroimaging